Radiology

Ronald Ouwerkerk, PhD
Karen B. Bleich, MD
Joseph S. Gillen, BS
Martin G. Pomper, MD, PhD
Paul A. Bottomley, PhD

Index terms:
Brain neoplasms, 10.363
Brain neoplasms, MR, 10.121413, 10.12143, 10.12145
Brain neoplasms, MR spectroscopy, 10.12145
Magnetic resonance (MR), sodium studies, 10.121413, 10.12143, 10.12145

Published online before print
10.1148/radiol.2272020483
Radiology 2003; 227:529–537

Abbreviations:
CSF = cerebrospinal fluid
FLAIR = fluid-attenuated inversion recovery
GM = gray matter
ROI = region of interest
TR = repetition time
WM = white matter
3D = three-dimensional

[1] From the Department of Radiology, Divisions of MR Research (R.O., K.B.B., J.S.G., P.A.B.) and Neuroradiology (M.G.P.), Johns Hopkins University School of Medicine, 610 N Caroline St, JHOC 4241, Baltimore, MD 21287-0845. From the 2001 RSNA scientific assembly. Received April 26, 2002; revision requested June 21; final revision received October 9; accepted October 14. Supported by National Institutes of Health grants R01HL061695, R21HL62332, and 1P41RR015241-01A1 and American Cancer Society grant IRS-58-005-40. **Address correspondence to** R.O. (e-mail: *rouwerke@mri.jhu.edu*).

Author contributions:
Guarantors of integrity of entire study, R.O., P.A.B.; study concepts, R.O., M.G.P., P.A.B.; study design, R.O., P.A.B., M.G.P., J.S.G.; literature research, R.O.; clinical studies, R.O., K.B.B., M.G.P.; experimental studies, R.O., K.B.B., J.S.G.; data acquisition, R.O., K.B.B.; data analysis/interpretation, R.O., M.G.P., P.A.B.; statistical analysis, R.O.; manuscript preparation, R.O.; manuscript definition of intellectual content, R.O., P.A.B., M.G.P.; manuscript editing, R.O., P.A.B.; manuscript revision/review, P.A.B., M.G.P.; manuscript final version approval, all authors.

Tissue Sodium Concentration in Human Brain Tumors as Measured with ^{23}Na MR Imaging[1]

PURPOSE: To use combined proton (^{1}H) and sodium 23 (^{23}Na) magnetic resonance (MR) imaging to noninvasively quantify total tissue sodium concentration and to determine if concentration is altered in malignant human brain tumors.

MATERIALS AND METHODS: Absolute tissue sodium concentration in malignant gliomas was measured on quantitative three-dimensional ^{23}Na MR images with tissue identification from registered ^{1}H MR images. Concentration was determined in gray matter (GM), white matter (WM), cerebrospinal fluid (CSF), and vitreous humor in 20 patients with pathologically proven malignant brain tumors (astrocytoma, $n = 17$; oligodendroglioma, $n = 3$) and in nine healthy volunteers. Sodium concentration in tumors and edema was determined from ^{23}Na image signal intensities in regions that were contrast material enhanced on T1-weighted ^{1}H images (tumors) or regions that were only hyperintense on fluid-attenuated inversion recovery (FLAIR) ^{1}H images (edema). Sodium concentrations were measured noninvasively from ^{23}Na images obtained with short echo times (0.4 msec) by using external saline solution phantoms for reference. Differences in mean sodium concentration of all healthy tissue and lesions in patients were tested with a paired *t* test. Concentration in uninvolved tissues in patients was compared with that in the same tissue types in the volunteers with an independent samples two-tailed *t* test.

RESULTS: Mean concentration (in millimoles per kilogram wet weight) was 61 ± 8 (SD) for GM, 69 ± 10 for WM, 135 ± 10 for CSF, 113 ± 14 for vitreous humor, 103 ± 36 for tumor, 68 ± 11 for unaffected contralateral tissue, and 98 ± 12 for FLAIR hyperintense regions surrounding tumors. Significant differences ($P < .002$) in sodium concentration were demonstrated by using a *t* test for both tumors and surrounding FLAIR hyperintense tissues versus GM, WM, CSF, and contralateral brain tissue.

CONCLUSION: ^{23}Na MR imaging with short echo times can be used to quantify absolute tissue sodium concentration in patients with brain tumors and shows increased sodium concentration in tumors relative to that in normal brain structures.

Sodium concentration is sensitive to disease as an indicator of cellular and metabolic integrity and ion homeostasis (1–6). Angiogenesis and cellular proliferation are important indicators of tumor malignancy. Changes in sodium/hydrogen (Na^+/H^+) exchange kinetics are part of the signaling mechanism that initiates cell division (7). Cell division and the acidic extracellular microenvironment of tumor cells are both associated with an increase in intracellular Na^+ concentration ($[Na^+]_{in}$). Increased $[Na^+]_{in}$ (4–6), increased Na^+/H^+ transporter activity (7), and altered (Na^+/K^+)-adenosine triphosphatase activity (8,9) have all been linked to tumor malignancy. In a recent study (10), investigators subcutaneously implanted a 9L glioma model in rats and indicated that successful chemotherapy can lead to normalization of the initially elevated sodium concentration as seen with conventional (single-quantum) and multiple-quantum ^{23}Na magnetic resonance (MR) spectroscopy.

Sodium 23 (^{23}Na) MR imaging of the human brain was performed about 15 years ago (11), but the intrinsically low signal-to-noise ratio of ^{23}Na MR imaging led to relatively

long imaging times and/or poor spatial resolution compared with those of proton (^{1}H) MR imaging. Those limitations, combined with the declining availability of broadband capability required for ^{23}Na MR imaging, restricted the use of ^{23}Na MR imaging to a few research sites. Interest in ^{23}Na MR imaging has been rekindled with the development of ultrashort echo time sequences (12) and hardware improvements (13,14) that permit better spatial resolution with shorter imaging times and better quantitative measurements of tissue sodium concentration. ^{23}Na MR imaging can now be performed in about 15 minutes, which allows it to be combined with a comprehensive ^{1}H MR imaging protocol. Prior ^{23}Na MR imaging findings showed elevated ^{23}Na signal intensities in brain tumors in mice (15), rats (16), and humans (17). In humans, elevated ^{23}Na signal intensities were found in edema and in gliomas but not in meningiomas (17). In patients with meningiomas, elevated ^{23}Na signal intensity was seen in the peritumoral parenchyma and was attributed to edema (17,18). An increase in ^{23}Na signal intensity was also reported in experimentally induced acute and chronic cerebral edema in dogs (18). Consequently, it is currently unclear whether the increase in ^{23}Na signal intensity in malignant tumors is significantly different from that in peritumoral edema. Therefore, to quantify and characterize tissue sodium concentration in tumors and to distinguish the results from those of peritumoral edema, it is important to combine ^{23}Na MR imaging with a method of discriminating between edema and tumor. Therefore, we used contrast agent–enhanced T1-weighted ^{1}H MR imaging and fluid-attenuated inversion recovery (FLAIR) MR imaging to define regions for quantification of tissue sodium concentration that are likely to represent tumor and edema.

The observed tissue sodium concentration is composed of the weighted average of extracellular sodium content ($[Na^+]_{ex}$) and $[Na^+]_{in}$ in the tissue being examined. $[Na^+]_{ex}$ at 140 mmol/L is typically much higher than is $[Na^+]_{in}$, which is about 10–15 mmol/L. Arguably, the more physiologically relevant information is in the intracellular component, reflecting the ability of the cell to pump out sodium ions, whereas $[Na^+]_{ex}$ will remain virtually constant as long as there is adequate perfusion to the tissue. When the relative contribution of the $[Na^+]_{in}$ to the tissue sodium concentration is large, as it is in brain tumors, the sodium concentration provides a measure of metabolic changes affecting $[Na^+]_{in}$. Estimates for the extracellular volume fraction in the brain vary from 6% to 20% (16). When one considers that tissue perfusion fixes the extracellular concentration at about 140 mmol/L, assuming a normal intracellular concentration of 12 mmol/L, it can be calculated that the contribution of $[Na^+]_{in}$ in normal tissue is between 26% and 57%. More than half of the combined ^{23}Na signal is due to intracellular ^{23}Na when the partial volume of the extracellular compartment is less than 7%. Thus, despite the inability to resolve intra- and extracellular components of the ^{23}Na signal, the measurement of sodium concentration is a sensitivity measure of $[Na^+]_{in}$.

The goal of the present study was to combine ^{1}H and ^{23}Na MR imaging to noninvasively quantify total tissue sodium concentration and to test whether concentration is altered in malignant human brain tumors.

MATERIALS AND METHODS

Participants

The ^{23}Na and ^{1}H MR imaging protocol was performed in 20 consecutive patients (12 men, mean age of 39 years ± 13 [SD] and age range of 25–65 years; eight women, mean age of 43 years ± 16 and age range of 16–67 years) with malignant brain tumors (astrocytoma, n = 17; oligodendroglioma, n = 3) that were pathologically proven prior to therapy or surgical intervention. An additional six patients underwent MR imaging but were omitted from the results because they had benign lesions (four meningiomas and two cysts). The protocol, excluding contrast–enhanced ^{1}H MR imaging, was also applied to nine healthy volunteers (six men, three women; age range, 22–63 years) who served as control subjects. The volunteers had no symptoms, no evidence of a lesion at MR imaging, and no history of brain tumors or other neurologic disease. Our institutional review board approved the study and required written informed consent from all volunteers prior to MR imaging.

MR Imaging

All MR imaging was performed with a commercially available 1.5-T MR imaging system (Signa Echo Speed on a 5.8 Epic platform; GE Medical Systems, Milwaukee, Wis) equipped with spectroscopic broadband capabilities and a gradient accelerator module. Gradient amplifiers were capable of generating waveforms with a maximum amplitude of 2.2 mT/m and a maximum slew rate of 120 mT/m/msec. Individuals were positioned supine with their heads in a cradle. The cradle allowed switching between a ^{1}H quadrature coil and a ^{23}Na quadrature head coil without moving the individual's head. The long axis of the ^{23}Na coil was centered 1–2 cm above the glabella to provide a reproducible radio-frequency (B_1) field. Two 2.7 × 10-cm tubes of sodium gel were placed parallel to the long axis of the coil on either side of the head to serve as concentration references and fiducial markers. The tubes contained 2% agarose gel made of 60- and 120-mmol/L NaCl solutions in deionized water, doped with 2 g/L $CuSO_4$. The automatic shimming routine of the MR imager was used to optimize the magnetic field homogeneity on the basis of the ^{1}H signal by using the body coil or the imager's 16-element quadrature ^{1}H head coil. In all patients, ^{23}Na MR imaging was performed prior to contrast-enhanced ^{1}H MR imaging to avoid any potential effects of residual contrast agent on the ^{23}Na images.

For quantitative measurements of tissue sodium concentration, corrections for saturation were applied, except where excitation with a 90° flip angle was used with a repetition time (TR) of more than three times the longest longitudinal T1. The ^{23}Na T1 in the human brain and the B1 field homogeneity of the ^{23}Na birdcage coil applied to the head were both mapped three dimensionally (3D), as described in the following sections.

^{23}Na MR Imaging

The ^{23}Na coil was a custom-built 16-element ^{23}Na birdcage coil tuned to 16.9 MHz and interfaced with a carbon 13 MR spectroscopy preamplifier and the broadband transmitter by means of a quadrature 90° phase-splitter circuit. A nonselective ^{23}Na free induction decay was used to center the spectrometer frequency to the ^{23}Na resonance and optimize the transmit gain for maximum signal intensity with a nominal 90° nonselective block pulse excitation of 0.4 msec. The transmit gain was fine tuned by adjusting it to achieve a signal null (a 180° flip angle) with an excitation pulse of twice the length (0.8 msec). A 3D twisted-projection imaging sequence with 1,240 projections on 22 cones in 3D k space was used with gradient strengths of up to 1.6 mT/m (12). The projections were oversampled by 1,796 points over 29 msec with the receiver bandwidth set to 31.25 kHz: The signal-to-noise ratio is determined by the effective bandwidth of

about 1.1 kHz that is obtained after regridding. To maximize detection of the short T2 component, the 0.4-msec 90° pulse was followed by a 0.17-msec gradient delay to yield an echo time of 0.37 msec. The images were recorded with a TR of 120 msec and an estimated specific absorption rate of 0.2 W/kg. Given the short T1 of sodium in brain tissues (10–30 msec), a TR of 120 msec corresponds to nearly fully relaxed conditions for normal brain tissue. Six signals were acquired for each of the 1,240 projections to give a total imaging time of 14 minutes 52 seconds. The raw image data were regridded to 64 × 64 × 64 k-space points and Fourier transformed to a final image size of 64 × 64 × 64 pixels with a field of view of 22 cm in all directions (12). The pixel size was 0.34 mm isotropically or 0.04 mL, but the empirically determined spatial resolution was about 0.2 mL isotropically (12).

Coil Sensitivity Mapping

The coil sensitivity was mapped by using the same ^{23}Na MR imaging protocol with varying transmitter gains, with the coil applied to the head of a healthy volunteer. The transmitter gain was first optimized for a nominal 90° pulse as described above, and ^{23}Na images were obtained. ^{23}Na MR imaging was then repeated with the transmitter gain increased and decreased by 3 dB to yield images with nominal (unlocalized) flip angles of 45°, 90°, and 135°. These images were reconstructed with matrix sizes reduced to 32 × 32 × 32 points. For points on images with intensities on the nominal 90° image that were above a threshold of 5% of the maximum intensity, the B1 field strength was determined with a nonlinear least squares fit of the intensities of the corresponding pixels k in all three images to a function relating the image intensity to the local coil receive and transmit sensitivities described in detail in the Appendix.

T1 Measurements

The T1 of brain tissue was measured in healthy volunteers with ^{23}Na twisted-projection MR imaging repeated with different TR values of 40, 85, and 120 msec, with 12, eight, and six signals acquired, respectively, to maintain imaging times of 11–15 minutes and nominal 90° flip angles. The images were processed as described above, scaled according to the number of signals acquired and the average signal intensity measured in manually prescribed regions of interest (ROIs) in gray matter (GM), white matter (WM), cerebrospinal fluid (CSF), and vitreous humor. T1 values were calculated from the average signal intensities (I_k) found in identical ROIs on all three images by using a nonlinear least squares fit to

$$I_k = A[1 - B \exp(-\mathrm{TR}/\mathrm{T1})] \qquad (1)$$

(Multifit for MacIntosh PowerPC; Day Computing, Cambridge, England) with constants A and B.

Quantification of Sodium Concentration

To ensure precise anatomic localization and radiologic evaluation of lesions, ^{1}H MR imaging was performed after ^{23}Na MR imaging. Contrast-enhanced (Magnevist; Berlex, Montville, NJ) MR imaging was clinically prescribed for most patients (n = 12) as part of their standard preoperative MR examination.

The ^{1}H MR examination consisted of a FLAIR (9,000/153/2,200 [TR msec/echo time msec/inversion time msec]) sequence, a full-brain T2-weighted fast spin-echo (6,000/95; echo train length, eight; 256 × 256 × 60 voxels at a 240 × 24 × 180-mm field of view) sequence, and a contrast-enhanced T1-weighted 3D spoiled gradient-echo sequence (1.2/2.1/300, 1.5-mm section thickness, 256 × 256 × 124 voxels at a 240 × 24 × 180-mm field of view). Finally, after manual bolus injection of 20 mL of contrast material, about 40 coronal and 30 sagittal fast spin-echo images were obtained (400/21; flip angle, 90°; 5-mm section width).

Data Processing

The reconstructed ^{23}Na and ^{1}H images were regridded to 128 × 128-pixel resolution and 32 or 64 sections and registered by matching their orientation and field of view with the full-brain T2-weighted 3D image set. The images were regridded by means of 3D linear interpolation in Matlab (Mathworks, Natick, Mass) by using header information from the gradient-echo MR image files to construct grids for the original and desired data point locations. For comparison of tumor and contralateral tissue, contrast-enhanced ^{1}H images were used to determine ROIs, which were projected onto the ^{23}Na MR images. The mean values and SDs of the pixel intensities in these contrast-enhanced ROIs were determined and labeled as tumor. Areas of hyperintensity on FLAIR images, excluding those regions that were contrast enhanced on ^{1}H images, represented tissues that probably contained edema and/or infiltrative tumor. Signal intensities in these regions were quantified on the ^{23}Na images as well. The ROIs for uninvolved contralateral tissue were created by mirroring the locations of the ROIs containing tumor in relation to the location of the central fissure, except for in patients in whom the tumor location or brain deformation prevented accurate positioning with this method. In those patients, the ROIs for uninvolved contralateral tissue were either placed manually or omitted. The mean ^{23}Na image signal intensities in GM, WM, CSF, and vitreous humor were quantified in ROIs that were independently and manually placed (R.O., M.G.P.). The result was that values from multiple sections were averaged for the various tissue types in each patient.

Correction factors for saturation for each pixel k, SF_k, were calculated with T1 and B1 values (in Teslas) determined from coil sensitivity mapping and T1 measurements (Eq [1]) as described in the Appendix.

The mean sodium concentration per kilogram wet weight in the kth ROI was then determined from

$$[\mathrm{Na}]_k = \frac{\dfrac{I_k}{R_k \cdot \mathrm{SF}_k} - b}{a \cdot D}, \qquad (2)$$

where R_k is the sensitivity of the coil in location k. The factor D is the tissue density in kilograms per liter. D was 1.038 kg/L for WM (19), 1.034 kg/L for GM, and 1.038 kg/L for tumor on the basis of no significant difference in water content or specific gravity between tumor and surrounding WM (19). The coefficients a and b were calculated from the sodium concentrations C_1 and C_2 and signal intensities I_1 and I_2 of the two phantoms as

$$a = \frac{\dfrac{I_2}{R_2 \cdot \mathrm{SF}_2} - \dfrac{I_1}{R_1 \cdot \mathrm{SF}_1}}{C_2 - C_1} \qquad (3)$$

and

$$b = \frac{I_2}{R_2 \cdot \mathrm{SF}_2} - a \cdot C_2, \qquad (4)$$

where R_1 and R_2 are sensitivity factors.

For calculations of mean sodium concentration in ROIs within the same transverse section, the sensitivity factors R_1 and R_2 were set to unity. The mean signal intensities of all phantom ROIs were plotted against transverse section position to determine sensitivity changes over the long axis of the coil. Because the signal intensity from the phantom with the

TABLE 1
^{23}Na Concentrations Measured with MR Imaging in Brain Tissues and Tumors

Study	No. of Study Subjects	Tumor	GM	WM	CSF	Vitreous Humor
Present study (patients)	20	104 ± 33	61 ± 9	71 ± 13	135 ± 11	112 ± 15
Present study (control subjects)	9	NA	60 ± 6	69 ± 11	135 ± 15	130 ± 18
Winkler et al, 1989 (20)	4	NA	69 ± 16	34 ± 7	109 ± 20	NA
Constantinides et al, 2000 (21)	3	NA	NA	43 ± 0.9	121 ± 0.5	NA
Summers et al, 1991 (15)	29	87 ± 29*	NA	NA	NA	NA
Goldsmith and Damadian, 1975 (1)	18	83–141†	NA	NA	NA	NA

Note.—Data are mean ^{23}Na concentrations (millimoles per kilogram wet weight) ± SD unless otherwise indicated. NA = not applicable.
* IMR-5 neuroblastoma in nude mice.
† Values are concentration range for Walker-256 carcinosarcoma (n = 5) and Novikoff hepatoma (n = 5) grown in rats and Ehrlich ascites tumor (n = 2) and sarcoma-180 (n = 6) grown in mice.

highest sodium concentration was always constant within 5% over 8 cm of its length, the sodium concentration for tissues within this region was calculated with Equations (2)–(4) by using the average phantom signal intensity over multiple sections. Sodium concentration was always determined by averaging the concentrations in ROIs from the same tissue types in multiple sections in each patient. If the sodium concentration in tumor or the eyes showed variations between sections that could be due to partial volume effects, data from these sections were omitted from the averages.

Statistical Analysis

All statistical analyses were performed with Analyse-It Excel add-in software (Analyse-It, Leeds, England). Sodium concentrations of different tissues within the patient group were tested with a paired two-tailed t test for the null hypothesis that the mean concentrations in the tissues were equal. Because the plasma sodium concentration is arguably the maximum achievable value of sodium concentration in lesions, it is conceivable that the concentration in lesions does not have a normal distribution around the means. To account for this, the sodium concentrations in contrast-enhanced lesions (tumor) and in FLAIR hyperintense nonenhanced regions surrounding tumors were also compared with the mean calculated concentrations in all unaffected tissues, including contralateral uninvolved tissue, by using a nonparametric Wilcoxon signed rank test.

For comparison of sodium concentrations in unaffected brain tissues of patients with brain tissue types similar to those of healthy volunteers, an independent samples two-tailed t test was used.

In all statistical comparison tests, the null hypothesis was that the sodium concentrations in the sample groups were equal with a significance cutoff level of .05. Thus, P values of .05 or less were deemed indicative of a significant difference between the means.

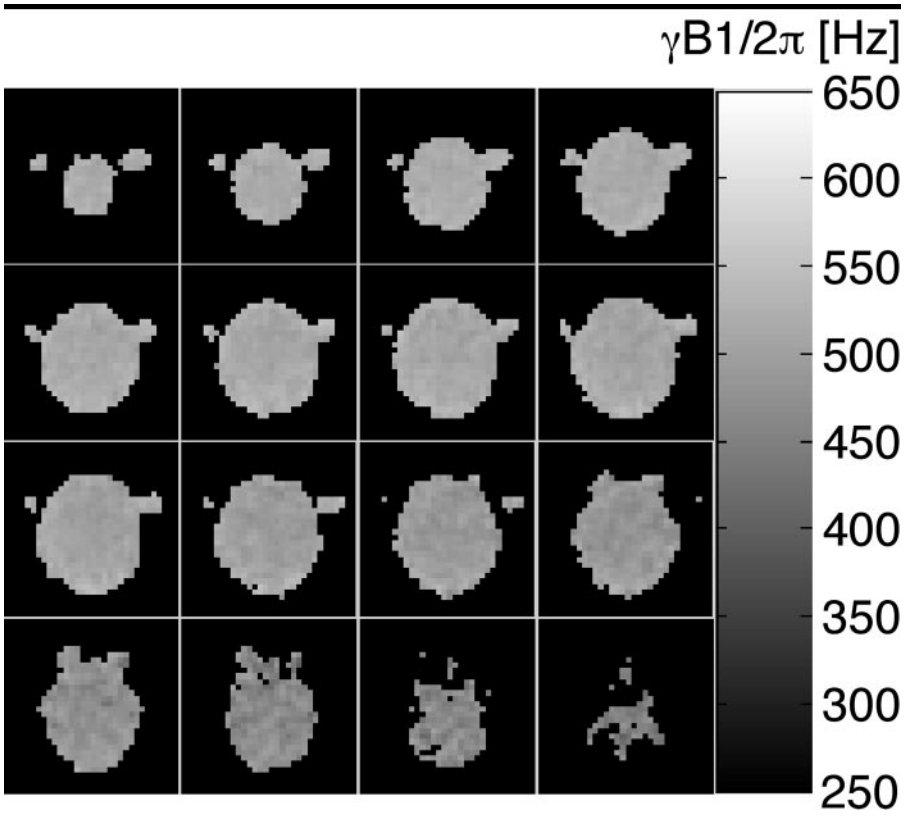

Figure 1. Sections from the 3D map of the B_1 field of the quadrature coil measured in the head of a healthy volunteer. Section spacing is 6.8 mm, and field of view is 22 × 22 × 11 cm. The shades of gray correspond to B_1 field strengths expressed in Hertz, as shown in the gray scale bar. The B_1 set on an unlocalized signal was 625 Hz, which corresponded to a 400-μsec block pulse width for a 90° flip angle.

RESULTS

A 3D coil sensitivity map calculated from data recorded in a healthy volunteer is shown in Figure 1. The map shows that the B_1 field strength in transverse planes (perpendicular to the long axis of the coil) is uniform within about ± 8%. With the nominal B_1 field strength ($\gamma B1/2\pi$) set to 625 Hz to generate a 90° flip angle for the observed bulk signal by using the 400-μsec block pulse as described in Materials and Methods, the B_1 field strength for the brain varies between 550 and 650 Hz along the long axis of the birdcage coil. However, it is essentially constant within transverse sections. The effect of

TABLE 2
^{23}Na Concentration in Tumors, Hyperintense Unenhanced Tissues, and Normal Tissues in Patients with Brain Tumors

Patient No.	Diagnosis	Lesion Location	Age (y)	Sex	Sodium Increase (%)* Tumor (n = 20)	Sodium Increase (%)* FHN (n = 12)	^{23}Na Concentration (mmol/kg wet weight) GM (n = 20)	WM (n = 20)	CSF (n = 19)	Tumor (n = 20)	Con (n = 18)	FHN (n = 12)	R VH (n = 20)	L VH (n = 19)
1	Oligodendroglioma, grade II	L temporal lobe	54	F	42	NA	51	63	128	88	62	NA	91	94
2	Oligodendroglioma, grade II	L basal ganglia	26	M	48	32	65	75	122	113	76	100	110	108
3	Astrocytoma, grade II	R temporal lobe	13	F	66	NA	64	68	127	106	94	NA	109	112
4	Astrocytoma, grade II	L temporal lobe	55	F	45	23	67	73	144	108	74	91	118	118
5	Astrocytoma, grade II	L posterior frontal lobe	28	M	40	NA	76	97	160	108	77	NA	124	121
6	Astrocytoma, grade II	Corpus callosum	39	F	26†	NA	75	86	142	39	NA	NA	127	119
7	Astrocytoma, grade III	L parietal lobe	51	M	66	43	56	57	146	94	56	81	134	135
8	Astrocytoma, grade III	R frontal lobe	46	M	49	67	53	64	122	88	59	99	95	113
9	Astrocytoma, grade III	R parietal lobe	36	M	31	43	69	83	145	98	75	107	114	119
10	Astrocytoma, grade III	R frontal lobe	41	M	25	NA	54	67	126	78	62	NA	107	109
11	Astrocytoma, grade III	L frontal lobe	41	M	63	51	78	95	182	155	103	102	124	NA
12	Astrocytoma, grade III	L frontal lobe	39	F	80	102	51	64	136	117	65	63	90	96
13	Astrocytoma, grade III	R temporal lobe	37	F	65†	NA	73	96	130	120	NA	NA	107	99
14	Oligodendroglioma, grade IV	R inferior frontal lobe	67	F	27	NA	71	88	140	105	83	NA	128	119
15	Astrocytoma, grade IV	R temporal lobe	39	F	35	39	67	71	144	102	75	104	136	136
16	Astrocytoma, grade IV	R parietotemporal lobe	40	M	58	42	78	110	NA	148	133	94	106	101
17	Astrocytoma, grade IV	R frontoparietal lobe	25	M	63	73	57	69	152	113	69	120	141	139
18	Astrocytoma, grade IV	L occipitoparietal lobe	65	M	43	NA	62	68	137	97	68	NA	98	90
19	Astrocytoma, grade IV	R occipital lobe	29	M	74	53	63	72	121	113	65	99	119	114
20	Astrocytoma, grade IV	L frontal lobe	37	M	77	42	48	53	128	104	59	83	102	94
Mean ± SD	···	···	···	···	51 ± 18	51 ± 21	64 ± 10	76 ± 15	139 ± 15	105 ± 24	75 ± 19	95 ± 14	114 ± 15	112 ± 14

Note.—Con = contralateral uninvolved tissue, FHN = FLAIR hyperintense nonenhanced tissue, GBM = glioblastoma multiforme, L = left, NA = not applicable, R = right, VH = vitreous humor (in right and left eyes).
* ^{23}Na increase with regard to contralateral tissue or GM.
† ^{23}Na increase in tumor relative to GM.

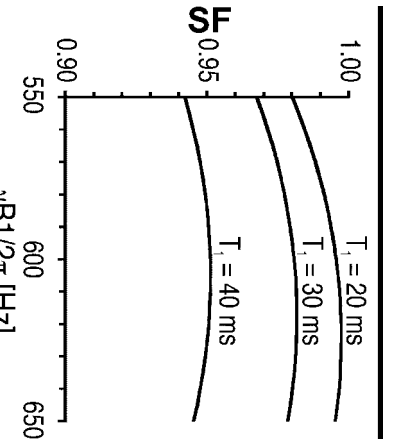

Figure 2. Graph shows combined effect of flip angle variations due to B_1 inhomogeneity and saturation calculated with Equation (A4) (Appendix) for the B_1 field range measured for the ^{23}Na coil applied to a volunteer's head (550 Hz < $\gamma B_1/2\pi$ < 650 Hz) for a T1 of 20, 30, and 40 msec and a TR of 120 msec.

the resulting variation in excitation pulse flip angle on the received signal is minimized when the TR ≫ T1. The T1 measurements in a healthy volunteer yielded values of 11.2 msec ± 0.4 for GM, 16.9 msec ± 0.3 for WM, 20 msec ± 2 for CSF, 26 msec ± 5 for vitreous humor, and 32 msec ± 5 for the $CuSO_4$-doped gel phantoms. In two volunteers and two patients, however, the ratio of the CSF signals for acquisitions with TRs of 85 and 120 msec was 1.08 ± 0.04, which corresponds to a T1 of about 40 msec but is not consistent with a T1 of 20 msec. The SF_k values calculated with Equation (A4) for tissues with T1s of 20, 30, and 40 msec at a TR of 120 msec are plotted in Figure 2. This shows that the combined effects of saturation and flip angle variations across the brain with a B_1 field strength ranging from 550 to 650 Hz are less than 6% for CSF or phantoms with T1s of 20–40 msec and less than 2% for GM and WM with a T1 shorter than 20 msec.

The normal sodium concentration in various tissues as determined from 11 ^{23}Na images in the brains of nine volunteers are listed in Table 1.

The diagnoses and quantitative sodium concentrations for 20 patients are summarized in Table 2. In every patient, a contrast-enhanced region was found. In every case, sodium concentration in tumor was considerably greater than that in uninvolved WM, GM, or contralateral tissue from the same patient. Mean concentration in tumor was comparable to values for vitreous humor but was 1.6-fold higher than that in GM, 1.4-fold higher than that in WM, and 1.4-fold

higher than that in contralateral tissue. Sodium concentration in tumor was about 25% lower than that in CSF. All patients had a contrast-enhanced region, but only 12 patients had a FLAIR hyperintense nonenhanced region large enough to quantify sodium concentration unambiguously. In nine of these patients, sodium concentration in the FLAIR hyperintense nonenhanced region was lower than that in the corresponding tumor, and overall, mean concentration in FLAIR hyperintense nonenhanced tissue was about 13% lower than that in tumor in the patient group as a whole. Representative ^{23}Na images from the 3D data sets acquired from all of the patients are shown in Figure 3. In each case, tumors appear as hyperintense regions. Figure 4 is a bar graph that summarizes mean sodium concentration levels for all the tissue types quantified, averaged for all individuals.

In some patients, heterogeneity of sodium concentration was observed within the tumor and/or FLAIR hyperintense nonenhanced regions surrounding tumor. This is exemplified in the sets of ^{1}H and ^{23}Na MR images in patient 15, a 39-year-old woman with a glioblastoma multiforme in the right parietotemporal lobe, as shown in Figure 5. The patient had extensive hyperintense regions surrounding the tumor (Fig 5a–5d). The ^{23}Na signal intensities in the ROI with FLAIR hyperintense nonenhanced tissue, as well as in the ROI with tumor, are variable (Fig 5e, 5f). The SD of the signal intensities within the FLAIR hyperintense nonenhanced regions in this patient was more than 20% of the mean. This is high when compared with the SDs found for signal intensities of less than 3% of the mean in WM and CSF regions. Visual inspection of the GM regions in Figure 5e and 5f shows the sodium concentration in GM to be nonuniform also, perhaps as a result of varying degrees of CSF and/or WM contamination. When averaged within the ROI used for quantification, however, the sodium concentration in GM was fairly uniform between transverse sections in the same individual. A plot of sodium concentrations in normal brain tissues and tumor from patient 5 is shown in Figure 6. The phantom signal intensities shown as crosses connected by a thick (120-mmol/L phantom) or thin (60-mmol/L phantom) line are almost constant, except for decrease in the signal intensity of the 120-mmol/L phantom beyond section number 43, corresponding to the tapered end of this phantom tube. The sodium concentration as a function of section position shows an almost (inverted) parabolic pattern in the tumor and eyes (vitreous humor).

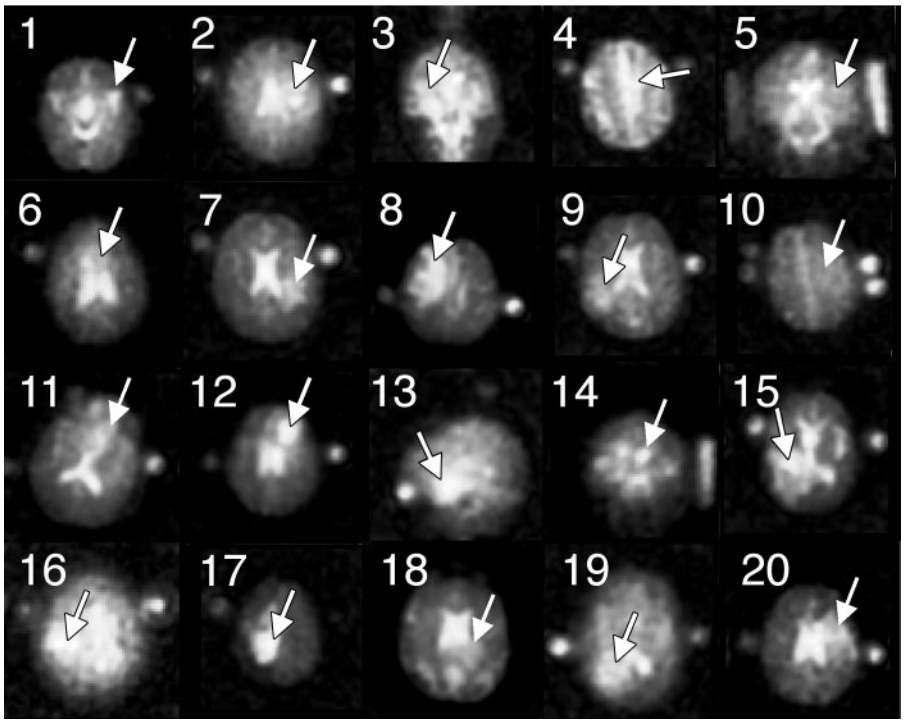

Figure 3. Selected sections from the 3D ^{23}Na MR images of all 20 patients listed in Table 2 with arrows indicating the position of the lesions. All sections were selected for maximal cross-sectional area through the tumor and are transverse sections except for those in patients 3, 5, and 14, for whom coronal sections are shown, and patient 13, for whom a sagittal section is shown.

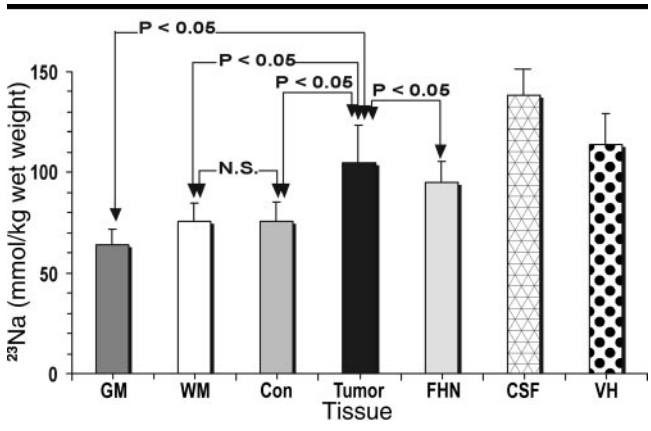

Figure 4. Average sodium concentration in GM, WM, CSF, tumor (contrast-enhanced hyperintense region), regions with edema or infiltrating tumor (*FHN* = FLAIR hyperintense nonenhanced region surrounding tumor), contralateral regions *(Con)* (relative to tumor), and vitreous humor *(VH)* in patients with gliomas.

Results of all statistical tests comparing sodium concentrations in tumor and other tissues are summarized in Table 3. By using a two-tailed paired samples *t* test, significant differences ($P < .002$) were demonstrated between tumor ($n = 20$) and uninvolved contralateral brain tissue ($n = 18$), tumor and GM ($P < .001$), tumor and WM ($P < .001$), and tumor and CSF ($P < .001$). The differences between tumor and surrounding FLAIR hyperintense nonenhanced regions ($n = 12$) were found at the .05 level of significance.

The Wilcoxon signed rank test yielded the same results with similar significance. Significant differences ($P < .002$) were

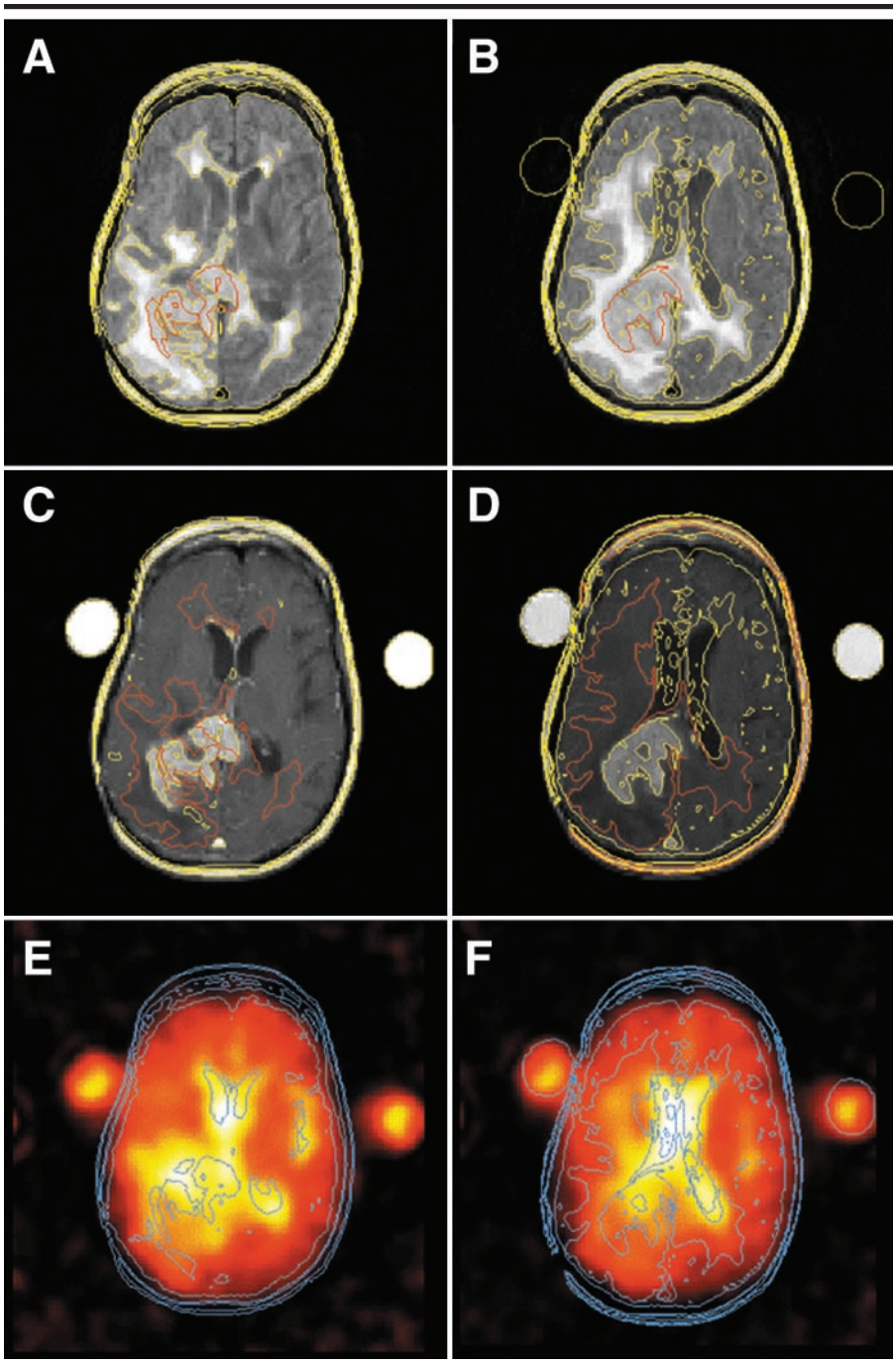

Figure 5. Patient 15. ^{1}H and ^{23}Na MR images in a 39-year-old woman with glioblastoma multiforme in the right temporal lobe. *A, B,* Transverse FLAIR MR images with level contours in yellow and contours from the matching contrast-enhanced images *C* and *D* superimposed in red. *C, D,* Contrast-enhanced T1-weighted MR images with level contours in yellow and FLAIR contours superimposed in red. *E, F,* ^{23}Na MR images with FLAIR and contrast-enhanced contours superimposed in blue.

found between tumor ($n = 20$) and FLAIR hyperintense nonenhanced regions ($n = 12$), tumor and GM ($P < .001$), tumor and WM ($P < .001$), and tumor and CSF ($P < .001$), while differences between tumor and surrounding FLAIR hyperintense nonenhanced regions ($n = 12$) were found at the .05 level of significance.

No statistically significant difference at the .05 level was found with use of a two-tailed independent samples *t* test between values for parenchymal brain tissues in patients compared with values for the same tissues in healthy volunteers.

DISCUSSION

The technique used for quantitative measurement of sodium concentration in brain tissues with use of external references yields reproducible results. The concentration calculated for GM is comparable to values observed previously with ^{23}Na MR imaging (20). The sodium concentration for CSF is higher than that observed previously with ^{23}Na MR imaging (20,21) but is in line with the value in the literature of 145.6 mmol/L ± 20.63, which was obtained with atomic absorption spectrometry (22). The sodium concentration found in vitreous humor is lower than the atomic absorption spectrometry value of 142 mmol/L in the literature (23).

The sodium concentration determined for GM agreed with prior ^{23}Na MR imaging measurements, whereas sodium concentration in WM is somewhat higher than that reported previously (20). This could be attributable to differences in the amount of partial volume contamination with CSF between the present study and the study of Winkler et al (20) as a result of differences in effective voxel size and/or geometry. The theoretical voxel size in the study of Winkler et al was $0.7 \times 0.7 \times 1.0$ cm, whereas the measured voxel size for the technique used in our study was 0.6 cm isotropically (12).

On the other hand, sodium concentration measured with the twisted-projection imaging sequence with ultrashort echo times in the present study is certain to be higher than values measured in previous studies in which spin- or gradient-echo MR sequences were used (20) because of the loss of signal intensity from the fast T2 component of in vivo ^{23}Na MR signals (24). The ^{23}Na signal in brain tissue exhibits biexponential transverse (T2) relaxation with fast and slow relaxing components in which fractions may also change with disease (25). The fast-relaxing component contributes up to 60% of the signal with a T2 in the range of 0.5–5.0 msec, depending on tissue type. The fastest ^{23}Na T2 value found in the literature for this component in human brain tissue is slightly more than 2.0 msec (21). Thus, for ^{23}Na MR imaging performed with echo times shorter than 0.4 msec in the present study, the maximum possible signal intensity loss is less than 10%. Any change in the ratio of the fast and slow relaxing components will reduce this signal loss even further. With an echo time of 2.0 msec or longer, such changes can have a much larger effect on signal intensity.

Thus, the differences in sodium content of GM and WM observed earlier with ^{23}Na MR imaging (26) may additionally reflect differences in relaxation components rather than changes in sodium concentration per se.

TABLE 3
***P* Values for ^{23}Na Concentrations in Brain Tissues**

Tissue Type	GM (n = 20)	WM (n = 20)	CSF (n = 20)	Tumor (n = 20)	Contralateral Tissue (n = 18)	FHN (n = 12)
GM (n = 20)	· · ·	<.002	<.001	<.001	<.01	<.001
WM (n = 20)	· · ·	· · ·	<.001	<.001	NS	<.002
CSF (n = 20)	· · ·	· · ·	· · ·	<.001	<.001	<.001
Tumor (n = 20)	· · ·	· · ·	· · ·	· · ·	<.001	NS
Contralateral tissue (n = 18)	· · ·	· · ·	· · ·	· · ·	· · ·	<.02
FHN (n = 12)	· · ·	· · ·	· · ·	· · ·	· · ·	· · ·

Note.—*P* values obtained with the paired *t* test. Significance cutoff was .05. FHN = FLAIR hyperintense nonenhanced tissue, NS = not significant.

Measurement of T1 confirmed that at a TR of 120 msec, the signals from brain tissues are nearly fully relaxed. Therefore, no corrections for saturation or flip angle were applied. The T1 determined for CSF was much shorter than the longest T1 of 90 msec reported in the literature (26). Even assuming that the T1 of CSF is about 40 msec, saturation has an almost negligible effect on the signal of CSF at a TR of 120 msec, as can be seen in Figure 2.

The high sodium concentration found in FLAIR hyperintense nonenhanced regions are consistent with findings in animal and human ^{23}Na MR imaging studies that show elevated sodium concentration in edema and in tumors (17,27). Findings in the present study demonstrate (noninvasively) in humans that the hyperintensity found in tumors and edema in earlier ^{23}Na MR imaging studies of brain tumors (17,27) is in fact a result of an increase in sodium concentration and is not entirely attributable to altered ^{23}Na relaxation times.

Although the observed sodium concentration reflects the sum of $[Na^+]_{in}$ and $[Na^+]_{ex}$, because $[Na^+]_{ex}$ in the blood pool is maintained essentially constant by the kidneys, the large increases seen here in tumors and edema likely reflect altered ion homeostasis. In particular, the almost 60% average increase in sodium concentration seen in tumors requires either a several-fold increase in $[Na^+]_{in}$ or a similar increase in extracellular volume fraction or a combination of both in these disease types. Assuming a normal $[Na^+]_{in}$ of 12 mmol/L and a normal extracellular volume fraction of 13%, the increase in $[Na^+]_{in}$ would have to be about 240%, or, conversely, at a constant $[Na^+]_{in}$, the extracellular volume fraction would have to increase by 380%.

Most likely, the increase in sodium concentration we observed in malignant tumors reflects both changes in extracellular volume fraction and in $[Na^+]_{in}$. Reduced (Na^+/K^+)–adenosine triphosphatase activity (6) and altered Na^+/H^+ exchange (28) kinetics that lead to increased $[Na^+]_{in}$ are associated with malignancy (6,29). Similarly, tumor neovascularization and increase in interstitial space both lead to increased extracellular volume fraction and are also associated with the potential for tumor proliferation. Therefore, sodium concentration levels in malignant tumors are likely to be elevated. From the clinical standpoint, the high sodium concentration in edema makes it imperative that quantification of sodium concentration in tumors is performed with the guidance of ^{1}H MR imaging with FLAIR and/or contrast-enhanced imaging sequences to help define abnormal regions. In the present study, the use of state-of-the-art receivers and coils and the twisted-projection imaging pulse sequence made it possible to collect 3D ^{23}Na images with good signal-to-noise ratio in less than 15 minutes, permitting use of combined ^{23}Na and ^{1}H MR imaging protocols with total examination times of about 45 minutes.

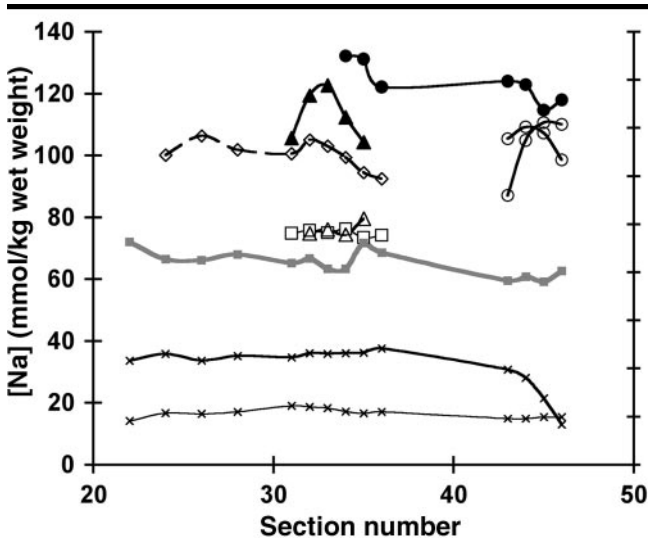

Figure 6. Patient 2. Graph shows sodium concentrations as a function of transverse section number (head to feet, with section spacing of 2.5 mm) for a 26-year-old man with oligodendroglioma. The two lowest traces are the phantom signal intensities on an arbitrary scale. All lines are spline fits to guide the eye. ■ = GM, □ = WM, △ = uninvolved contralateral brain tissue, ◇ = FLAIR hyperintense nonenhanced tissue (edema and/or infiltrating tumor), ▲ = tumor, ○ = vitreous humor, ● = CSF. Crosses connected by a thin (bottom trace, 60-mmol/L NaCl phantom) and a thick (top trace, 120-mmol/L NaCl phantom) line indicate signal intensities for the phantoms in arbitrary units (axis on right).

The heterogeneity of sodium concentration observed within FLAIR hyperintense contrast-enhanced regions and within FLAIR hyperintense nonenhanced regions suggests that ^{23}Na MR imaging may add information to a comprehensive ^{1}H MR examination. Because our ^{1}H MR imaging data provided no objective criteria to subdivide the tumor regions, however, sodium concentration was averaged over the surgically relevant contrast-enhanced regions. However, the increase in sodium concentration averaged for all contrast-enhanced regions may obscure the presence of even higher sodium concentration in proliferating parts and lower sodium concentration in dormant or slow-growing regions of tumor. Similarly, averaging sodium concentration for FLAIR hyperintense nonenhanced regions disregards the heterogeneity of sodium concentration in these regions, which could be indicative of the pres-

ence of infiltrating tumor rather than edema. Thus, one difficulty in further differentiating these regions is the lack of other suitable noninvasive imaging approaches that may be used as a standard of reference in human patients.

In conclusion, measurements of sodium concentration with ^{23}Na MR imaging can help identify malignant tumors with regard to the intrinsic changes that occur in tumor Na^+/K^+ pump function. Therapies that alter tumor ion homeostasis or affect or destroy tumor cell membrane integrity are likely to generate changes that are observable with ^{23}Na MR imaging and sodium concentration measurements. With these measurements, changes can be observed much earlier than the effects of anatomic remodeling. Therefore, these techniques may prove useful in providing early noninvasive metabolic markers of tumor response to therapy without requiring exogenous contrast-enhanced or radionuclide imaging agents. When used in conjunction with ^{1}H MR imaging protocols such as the FLAIR sequence, MR imaging contrast agents, and T2-weighted imaging methods, ^{23}Na MR imaging may provide additional functional information on the morphology of tumors that may enhance visualization of a necrotic core or proliferating periphery or improve diagnostic specificity with multiparametric analysis methods.

APPENDIX

Coil Sensitivity Mapping

The relationship between signal intensity and coil transmit and receive sensitivity used for coil sensitivity mapping was

$$I_k = R_k \cdot M_{0k} \cdot |\sin(\phi_k)|, \qquad \text{(A1)}$$

where I_k is the signal intensity of the kth pixel, R_k is a sensitivity factor to account for coil sensitivity variations that are normalized to the sensitivity at the coil center, M_{0k} is the equilibrium magnetization, and ϕ_k is the flip angle, which is determined from the empirical relation between transmitter gain setting TG (in decibels):

$$\phi_k = (C \cdot R_k) \cdot 10^{TG/20}. \qquad \text{(A2)}$$

$(C \cdot R_k)$ and M_{0k} were each fitted with a single parameter for each pixel. The constant C is independent of spatial position, and receive sensitivity is directly proportional to transmit field distribution for the coil. After normalization, the product $(C \cdot R_k)$ thus yields the relative sensitivity R_k for the kth pixel. The B_1 field strength, expressed as $\gamma B_1/2\pi$ in Hertz, was calculated from the reference transmit power, Tgref, at which an unlocalized 90° excitation is achieved by means of

$$\frac{\gamma B_{1k}}{2\pi} = (C \cdot R_k) \cdot 10^{TGref/20}/(tp \cdot 2\pi), \qquad \text{(A3)}$$

where tp is the pulse duration (400 μsec).

Correction for Saturation and Coil Sensitivity

The correction factor SF_k to adjust signal intensity in a pixel or region k for effects of saturation and local coil sensitivity was calculated from the local B_1 field B_{1k} and the tissue T1 as

$$SF_k = \frac{[-e^{-TR/T1}] \cdot \sin\left(tp \frac{\gamma B_{1k}}{2\pi}\right)}{\left[1 - e^{-TR/T1} \cdot \cos\left(tp \frac{\gamma B_{1k}}{2\pi}\right)\right]}, \qquad \text{(A4)}$$

where B_{1k} is the B_1 field in the respective ROI and γ is the gyromagnetic ratio for ^{23}Na. The pulse time tp was always 0.4 msec, and the TR was always 120 msec.

Acknowledgment: The authors thank Fernando Boada, PhD, of the University of Pittsburgh for providing the original twisted-projection imaging pulse sequence used in this article.

References

1. Goldsmith M, Damadian R. NMR in cancer. VII. Sodium-23 magnetic resonance of normal and cancerous tissues. Physiol Chem Phys 1975; 7:263–269.
2. Doohan MM, Rasmussen HH. Myocardial cation transport. J Hypertens 1993; 11:683–691.
3. Negendank W. Studies of human tumors by MRS: a review. NMR Biomed 1992; 5:303–324.
4. Cameron IL, Smith NKR, Pool TB, Sparks RL. Intracellular concentration of sodium and other elements as related to mitogenesis and oncogenesis in vivo. Cancer Res 1980; 40: 1493–1500.
5. Ng KH, Bradley DA, Looi LM. Elevated trace element concentrations in malignant breast tissues. Br J Radiol 1997; 70:375–382.
6. Nagy I, Lustyik G, Lukacs G, Nagy V, Balazs G. Correlation of malignancy with the intracellular Na+:K+ ratio in human thyroid tumors. Cancer Res 1983; 43:5395–5402.
7. Rotin D, Steele-Norwood D, Grinstein S, Tannock I. Requirement of the Na+/H+ exchanger for tumor growth. Cancer Res 1989; 49:205–211.
8. Spector M, O'Neal S, Racker E. Phosphorylation of the beta subunit of Na+K+-ATPase in Ehrlich ascites tumor by a membrane-bound protein kinase. J Biol Chem 1980; 255:8370–8373.
9. Kasarov LB, Friedman H. Enhanced Na+-K+-activated adenosine-triphosphatase activity in transformed fibroblasts. Cancer Res 1974; 34:1862–1865.
10. Winter PM, Poptani H, Bansal N. Effects of chemotherapy by 1,3-bis(2-chloroethyl)-1-nitrosourea on single-quantum- and triple-quantum-filtered Na-23 and P-31 nuclear magnetic resonance of the subcutaneously implanted 9L glioma. Cancer Res 2001; 61: 2002–2007.
11. Hilal SK, Maudsley AA, Ra JB, et al. In vivo NMR imaging of sodium-23 in the human head. J Comput Assist Tomogr 1985; 9:1–7.
12. Boada FE, Gillen JS, Shen GX, Chang SY, Thulborn KR. Fast three dimensional sodium imaging. Magn Reson Med 1997; 37:706–715.
13. Lee RF, Giaquinto R, Constantinides C, Souza S, Weiss RG, Bottomley PA. A broadband phased-array system for direct phosphorus and sodium metabolic MRI on a clinical scanner. Magn Reson Med 2000; 43:269–277.
14. Shen GX, Boada FE, Thulborn KR. Dual-frequency, dual-quadrature, birdcage RF coil design with identical B1 pattern for sodium and proton imaging of the human brain at 1.5 T. Magn Reson Med 1997; 38:717–725.
15. Summers RM, Joseph PM, Kundel HL. Sodium nuclear magnetic resonance imaging of neuroblastoma in the nude mouse. Invest Radiol 1991; 26:233–241.
16. Thulborn KR, Davis D, Adams H, Gindin T, Zhou J. Quantitative tissue sodium concentration mapping of the growth of focal cerebral tumors with sodium magnetic resonance imaging. Magn Reson Med 1999; 41: 351–359.
17. Hashimoto T, Ikehira H, Fukuda H, et al. In vivo sodium-23 MRI in brain tumors: evaluation of preliminary clinical experience. Am J Physiol Imaging 1991; 6:74–80.
18. Turski PA, Perman WH, Hald JK, Houston LW, Strother CM, Sackett JF. Clinical and experimental vasogenic edema: in vivo sodium MR imaging—work in progress. Radiology 1986; 160:821–825.
19. Takagi H, Shapiro K, Marmarou A, Wisoff H. Microgravimetric analysis of human brain tissue: correlation with computerized tomography scanning. J Neurosurg 1981; 54: 797–801.
20. Winkler SS, Thomasson DM, Sherwood K, Perman WH. Regional T2 and sodium concentration estimates in the normal human brain by sodium-23 MR imaging at 1.5 T. J Comput Assist Tomogr 1989; 13:561–566.
21. Constantinides CD, Boada F, Bolar D, Gillen J, Pomper MG. Sodium MRI in cancer at 1.5 T (abstr). In: Proceedings of the Eighth Meeting of the International Society for Magnetic Resonance in Medicine. Berkeley, Calif: International Society for Magnetic Resonance in Medicine, 2000; 387.
22. Walther LE, Streck S, Winnefeld K, Walther BW, Kolmel HW, Beleites E. Reference values for electrolytes (Na, K, Ca, Mg) and trace elements (Fe, Cu, Zn, Se) in cerebrospinal fluid. Trace Elem Electrolytes 1998; 15:177–180.
23. Naumann HN. Postmortem chemistry of the vitreous body in man. Arch Ophthalmol 1959; 62:356–363.
24. Boada FE, Christensen JD, Huang-Hellinger FR, Reese TG, Thulborn KR. Quantitative in vivo tissue sodium concentration maps: the effects of biexponential relaxation. Magn Reson Med 1994; 32:219–223.
25. Kalyanapuram R, Seshan V, Bansal N. Three-dimensional triple-quantum-filtered 23Na imaging of the dog head in vivo. J Magn Reson Imaging 1998; 8:1182–1189.
26. Feinberg DA, Crooks LA, Kaufman L, et al. Magnetic resonance imaging performance: a comparison of sodium and hydrogen. Radiology 1985; 156:133–138.
27. Schuierer G, Ladebeck R, Barfuss H, Hentschel D, Huk WJ. Sodium-23 imaging of supratentorial lesions at 4.0 T. Magn Reson Med 1991; 22:1–9.
28. Lagarde AE, Pouyssegur JM. The Na+:H+ antiport in cancer. Cancer Biochem Biophys 1986; 9:1–14.
29. Cameron IL, Hunter K. An x-ray-microanalysis study on the progressive increase in intracellular sodium concentration associated with DMH induction of colon cancer (abstr). Proceedings of the American Association For Cancer Research, 1984; 25:131.